The Astrophysical Journal, 860:128 (7pp), 2018 June 20 https://doi.org/10.3847/1538-4357/aac496

Detection of Magnetic Nulls around Reconnection Fronts

C. M. Liu[1], H. S. Fu[1], D. Cao[1], Y. Xu[1], and A. Divin[2]

[1] School of Space and Environment, Beihang University, Beijing, People's Republic of China; hsfu@buaa.edu.cn

[2] Physics Department, St. Petersburg State University, St. Petersburg 198504, Russia

Received 2018 March 29; revised 2018 May 11; accepted 2018 May 11; published 2018 June 20

Abstract

Magnetic nulls, where magnetic-field strength becomes zero, play a crucial role in energy conversion and particle acceleration during magnetic reconnection. Recent simulations have suggested that reconnection fronts (RFs) inside the reconnection jet can host magnetic nulls. However, observational evidence for the RF-associated magnetic nulls remains absent so far. In this study, we present such evidence by using the first-order Taylor expansion method and *Cluster* measurements. We confirm for the first time the existence of magnetic nulls around RFs, and find that the dip region ahead of RFs and the nearby magnetic flux ropes around RFs can be host to magnetic nulls. The observed magnetic nulls are all spiral types, and the reconstructed topologies are consistent with theoretical models. Our results verify the existence of magnetic nulls around RFs, and may shed new light on the study of magnetic reconnection and RF dynamics.

Key words: magnetic reconnection – turbulence

1. Introduction

Magnetic nulls, where the magnetic field disappears and particles get demagnetized, are stable structures, typically observed inside magnetic reconnection diffusion region. They have been suggested to be favorable places for electromagnetic energy conversion and particle acceleration in space plasma (Dalla & Browning 2006; Petkaki & MacKinnon 2007; Olshevsky et al. 2013, 2015; Fu et al. 2017). To date, wave characteristics and particle dynamics around magnetic nulls have been well studied by using spacecraft observations and numerical simulations (Parnell et al. 1997; Xiao et al. 2006; Pontin & Galsgaard 2007; He et al. 2008; Deng et al. 2009; Eriksson et al. 2015; Olshevsky et al. 2016; Chen et al. 2018). However, some important physical processes in association with the 3D characteristics of magnetic nulls still remain poorly understood (Fu et al. 2015, 2016). In particular, magnetic reconnection—a fundamental process converting magnetic energy into particle thermal and kinetic energy (Yamada et al. 2010, and references therein)—often occurs at magnetic nulls in the 3D regime (Priest & Titov 1996; Parnell et al. 2010; Pontin et al. 2005).

Magnetic reconnection was frequently observed in Earth's magnetosphere (Øieroset et al. 2001; Eastwood et al. 2010). It is the key process that facilitates the interaction between the solar wind and Earth's magnetosphere (Hasegawa et al. 2010), releases the stored magnetic energy in the magnetotail (Angelopoulos et al. 2013), and energizes the magnetospheric plasma (Øieroset et al. 2002). One important consequence of magnetic reconnection in the tail is the generation of reconnection front (RF) (Sitnov et al. 2009; Fu et al. 2013a), which is characterized by the sharp increase of magnetic field B_z (Nakamura et al. 2002; Runov et al. 2009; Fu et al. 2012a), and is usually embedded in the reconnection jet or bursty bulk flow (Cao et al. 2006). RF has been suggested to be the crucial region for suprathermal electron acceleration (Fu et al. 2011, 2013b; Liu et al. 2017b; Xu et al. 2018), wave-particle interactions (Zhou et al. 2009; Khotyaintsev et al. 2011; Fu et al. 2014), pitch angle evolution (Fu et al. 2012b; Liu et al. 2017a, 2017c), and electromagnetic energy conversion (Lapenta et al. 2014; Huang et al. 2015a; Yao et al. 2017; Liu et al. 2018) in the tail.

RF is a thin current sheet host to highly twisted magnetic field lines and sharp plasma gradients (Sitnov et al. 2009; Fu et al. 2012c), which may lead to the development of kinetic-scale instabilities (Pritchett et al. 2014; Divin et al. 2015). Recent simulations have suggested that these instabilities can provide the potential for the occurrence of magnetic nulls (Huang et al. 2015b; Lapenta et al. 2015). However, observational evidence for the occurrence of RF-associated magnetic nulls remains absent so far. As magnetic nulls can play a crucial role in particle acceleration, energy conversion, and triggering secondary reconnection, investigating the occurrence and properties of magnetic nulls associated with RFs is critically important. In this paper, we present such observational investigation for the first time, by using the first-order Taylor expansion (FOTE) method (Fu et al. 2015, 2016) and *Cluster*'s measurements in 2003 when the satellite constellation has a small separation (∼200 km, typically less than 0.5 d_i, where $d_i = c/\omega_{pi}$ is the ion inertial length, and ω_{pi} is the proton plasma frequency), with particular focus on their occurrence, properties, and topological structure. We illustrate data and method we use in Section 2, present case studies in Section 3, and finally give our conclusion in Section 4.

2. Data and Method

Because the separations among the *Cluster* spacecraft were ∼100–300 km in its 2003 tail season, multipoint observations of RFs allow us to study the surrounding magnetic nulls at subproton scale. We use the same RFs list of Fu et al. (2012a), which includes 41 RF events in 2003. Data from the FluxGate Magnetometer instrument, which provides 22 Hz magnetic-field data, and the *Cluster* Ion Spectrometry instrument, which provides 0.25 Hz ion data, are used in this study. All of the data are shown in the Geocentric Solar Magnetospheric coordinate system unless stated otherwise.

We use the FOTE (Fu et al. 2015, 2016) to detect magnetic nulls and investigate their properties. This method is based on a

Taylor expansion around a null:

$$\boldsymbol{B}(\boldsymbol{r}) = (\boldsymbol{r} - \boldsymbol{r}_n) \cdot \nabla \boldsymbol{B}, \tag{1}$$

where $\boldsymbol{r}$ is the satellite location in space, $\boldsymbol{B}$ is the magnetic field at $\boldsymbol{r}$, $\boldsymbol{r}_n$ is the null's location, and $\nabla \boldsymbol{B}$ is the gradient of magnetic field computed from the four-spacecraft measurements, assuming that the magnetic-field changes linearly in space. Compared with the previously used Poincare index method (Xiao et al. 2006; Deng et al. 2009), the FOTE method has several advantages in studying magnetic nulls (Fu et al. 2015). (1) It can avoid the limitations of data resolution, SC separation, and instruments uncertainty. (2) It can identify 3D magnetic null types by analyzing three eigenvalues of the jacobian matrix $\nabla \boldsymbol{B}$, such as A (radial null with one positive and two negative real eigenvalues), B (radial null with two positive and one negative real eigenvalues), As (spiral null with one positive real eigenvalue and two conjugate complex eigenvalues) and Bs (spiral null with one negative real eigenvalue and two conjugate complex eigenvalues). (3) It can reconstruct the magnetic topology. However, as the FOTE method can always find magnetic nulls, results of this method should be further diagnosed. In addition to the two error parameters (η and ξ, for quantifying the quality of the FOTE results) suggested by Fu et al. (2015), we introduce two additional restrictions to get reliable results, including (1) the null-satellite distance should be less than 0.5 d_i and (2) the detected null type should keep steady during observation (Eriksson et al. 2015). We treat results of FOTE method as reliable when these conditions are satisfied.

3. Case Overviews

Based on the RFs list of Fu et al. (2012a) and the FOTE method, we have classified six cases as RF-associated magnetic null events which clearly display the occurrence of magnetic nulls near the RFs. We find that the dip region ahead of RF and the nearby magnetic flux ropes around RFs can become host to magnetic nulls. To illustrate this, we present in this section three cases which show observations of magnetic nulls located in the dip region ahead of RF, magnetic flux ropes before and behind RF, respectively.

We first present observations of a magnetic null that is located inside the dip region ahead of a RF detected by *Cluster* on 2003 July 25, as shown in Figure 1. Figures 1(a)–(d) present the four-spacecraft observations of the magnetic field from 06:56:50 to 06:57:20 UT. Because the separations among the *Cluster* spacecraft were quite small, the four spacecraft provided very similar data. The magnetic field was dominated by B_z component (Figures 1(a)–(d)), with $|B_x| < 5$ nT, indicating that the spacecraft were located in the neutral sheet. Before 06:57:02 UT, the magnetic field was roughly steady (Figures 1(a)–(d)). A RF, characterized by abrupt increase of B_z (from 1 to 18 nT, Figure 1(a)) and decrease of ion density (not shown), was observed at ∼06:57:02.5 UT. The RF was embedded in a BBF with maximum velocity approaching 400 km s^{-1} (not shown). Through timing analysis, we determine the propagation velocity of the RF as 365*(0.99, −0.09, −0.07) km s^{-1}, which indicates that the spacecraft crossed the central part of the RF. Based on the RF duration (∼0.9 s), the thickness of the RF is about 329 km or equivalently 1 d_i, comparable to the typical RF thickness in the magnetotail (Fu et al. 2012a). The RF has a clear dip structure with minimum magnetic-field strength approaching 0 nT (at ∼06:57:02.2 UT, see Figure 1(d)), which is accompanied by reversal of B_x and B_y (Figures 1(b)–(c)). The dip region thus provides the potential for the nulls' existence. To investigate whether magnetic nulls exist inside the dip region, we apply the FOTE method on the magnetic-field data from 06:57:01 to 06:57:03 UT.

Figures 1(e)–(h) present the FOTE results, including (e) null-SC distance, (f) the minimum null-SC distance with types labeled, and (g, h) two parameters, η and ξ, for quantifying the quality of the FOTE results. As can be seen, distance between the null and the spacecraft is very small from 06:57:02.10 to 06:57:02.55 UT (Figure 1(e)), with the minimum distance (null-C4) approaching 85 km (less than 0.3 d_i). This null shows steady As type (Figure 1(f)), which may correspond to a magnetic flux rope structure. Considering that the two error parameters are generally small (Figures 1(g)–(h)), the As null detected from 06:57:02.10 to 06:57:02.55 UT should be reliable. Duration of the As null was ∼0.45 s, thus its spatial scale was ∼164 km (close to 0.5 d_i). Such sub-ion scale magnetic null may affect the RF magnetic-field structure. Note that a Bs null is also detected between 06:57:01.85 and 06:57:01.95 UT. However, we treat it as unreliable since the minimum null-SC distance (∼250 km, about 0.8 d_i) is larger than 0.5 d_i.

Recent simulations and observations have suggested that magnetic flux ropes and RFs may frequently appear together (Lu et al. 2015; Wang et al. 2017). It has also been suggested that flux ropes and structures (e.g., conjoined flux ropes) arising from the interactions between them can be host to magnetic nulls (Wyper & Pontin 2014a, 2014b; Titov et al. 2017). Therefore, the nearby flux ropes around RFs may also provide the potential for the occurrence of magnetic nulls. Figure 2 shows observations of magnetic null located inside a magnetic flux rope before a RF which was observed by *Cluster* on 2003 September 1. The cluster spacecraft were located in the neutral sheet ($|B_x| < 5$ nT, see Figure 2(b)). As can be seen, the magnetic flux rope, indicated by the change of B_z from 6 to −2 nT (Figure 2(a)), was observed from 02:16:00 to 02:16:16 UT. The flux rope has a weak core field (∼5 nT, see Figure 2(c)). The RF is detected at ∼02:16:18 UT when B_z increases sharply from 0 to 11 nT (Figure 2(a)). The RF and the flux rope appear very close to each other thus may have mutual interaction. Through timing analysis, however, we find that propagation velocity of the magnetic flux rope was 275*(0.69, 0.72, −0.02) km s^{-1}, approximately same as the propagation velocity of the RF, suggesting that these two structures move together toward the Earth without mutual compression or traction. Considering duration of the magnetic flux rope (∼16 s), its spatial scale was about 4400 km or equivalently 10.5 d_i. Note that from 02:16:11 to 02:16:16 UT, reversal of B_x and B_y is observed in region between the RF and the trailing edge of the flux rope, indicating possible occurrence of magnetic nulls in this region.

We perform the Taylor expansion on the interested interval from 02:16:11 to 02:16:16 UT, as displayed in Figures 2(e)–(h). We find that distance between the null and the spacecraft were quite small from 02:16:12.40 to 02:16:14.00 UT (Figure 2(e)), with the minimum distance (null-C4) approaching 30 km (∼0.07 d_i). Such small distance indicates that the spacecraft may cross the central region of the magnetic null. This null

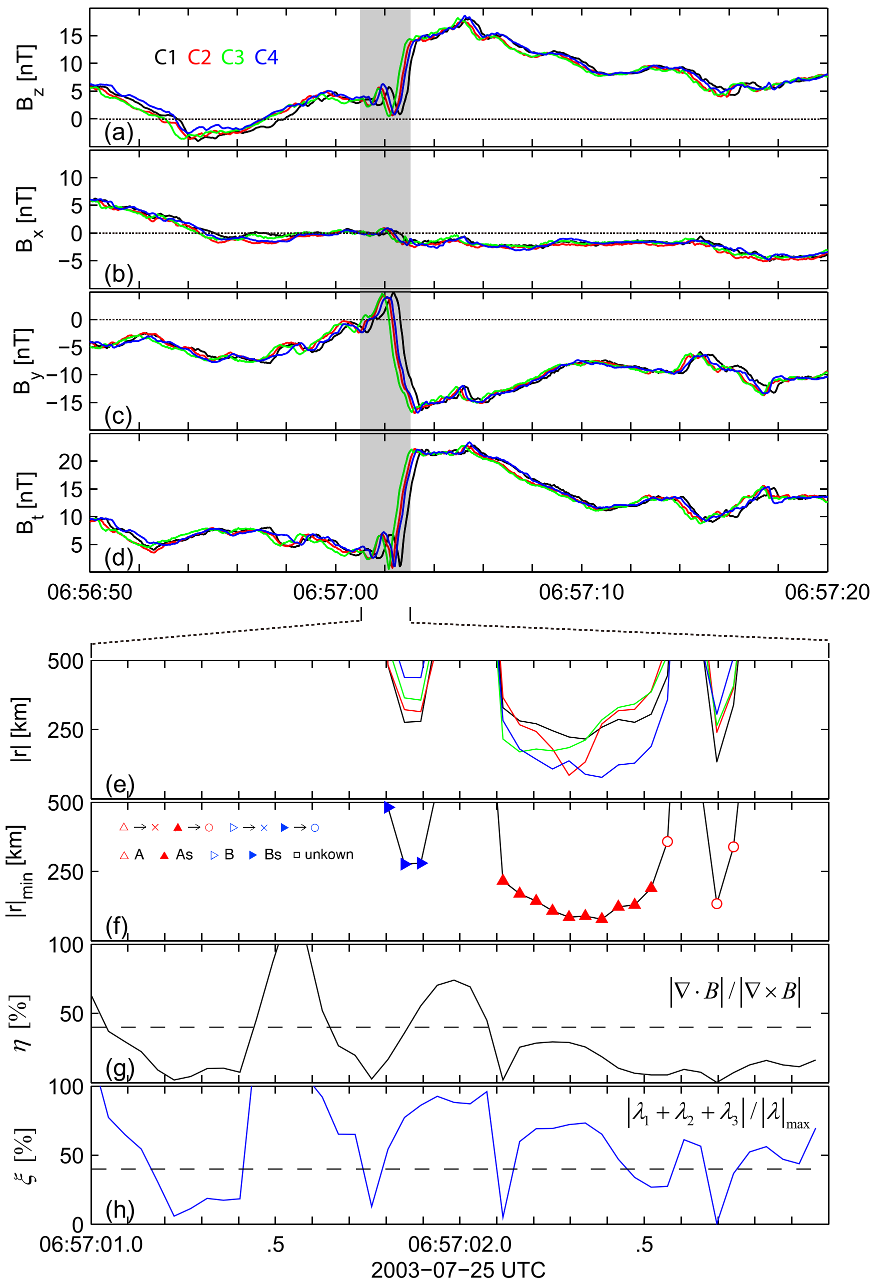

Figure 1. *Cluster* observations of magnetic null in the dip region ahead of a RF: (a) magnetic field B_z component; (b) magnetic field B_x component; (c) magnetic field B_y component; (d) the strength of the magnetic field; (e) null-SC distance; (f) the minimum null-SC distance with null types labeled; (g), (h) two parameters, η and ξ, for quantifying the quality of the FOTE results. The color lines describe the measurements of C1 (black), C2 (red), C3 (green), and C4 (blue). The dashed lines represent the zero levels of magnetic-field components.

presents steady Bs type, with the parameters η and ξ being generally small (Figures 2(g)–(h)). Therefore, this Bs null should be reliable. Considering duration of the Bs null ($\sim$1.6 s), its spatial scale was thus about 440 km ($\sim$1 d_i), close to the RF scale ($\sim$0.9 d_i).

We further present observations of multiple magnetic nulls located inside a magnetic rope behind a RF which was detected on 2003 September 29, as displayed in Figure 3. The RF structure was observed at $\sim$10:18:39 UT, characterized by dramatic increase of B_z (from 5 to 11 nT, see Figure 3(a)). The RF was embedded in a BBF with maximum speed approaching 800 km s^{-1} (not shown). A magnetic flux rope characterized by the bipolar change of B_z (from 5 to -4 nT, see Figure 3(a)) was detected from 10:19:12 to 10:19:23 UT. Propagation velocity of the magnetic flux rope derived from timing analysis is 241*(0.27, 0.41, 0.87) km s^{-1}. Considering duration ($\sim$11 s) of the flux rope, its spatial scale is about 2651 km or equivalently 5.2 d_i. Note that in the front edge of the magnetic flux rope (from 10:19:12 to 10:19:15 UT), observations by the four spacecraft are quite different, indicating that magnetic-field structure in this region has a scale well below the spacecraft separation. During this interval, C1 crossed the central current sheet and observed reversal of B_y, suggesting that C1 may encounter magnetic null structures.

We perform the FOTE analysis on the interested interval, as shown in Figures 3(e)–(h). As can be seen, the estimated distance between null and spacecraft were quite small during three intervals: 10:19:12.45–10:19:12.85 UT, 10:19:12.90–10:19:13.35 UT, and

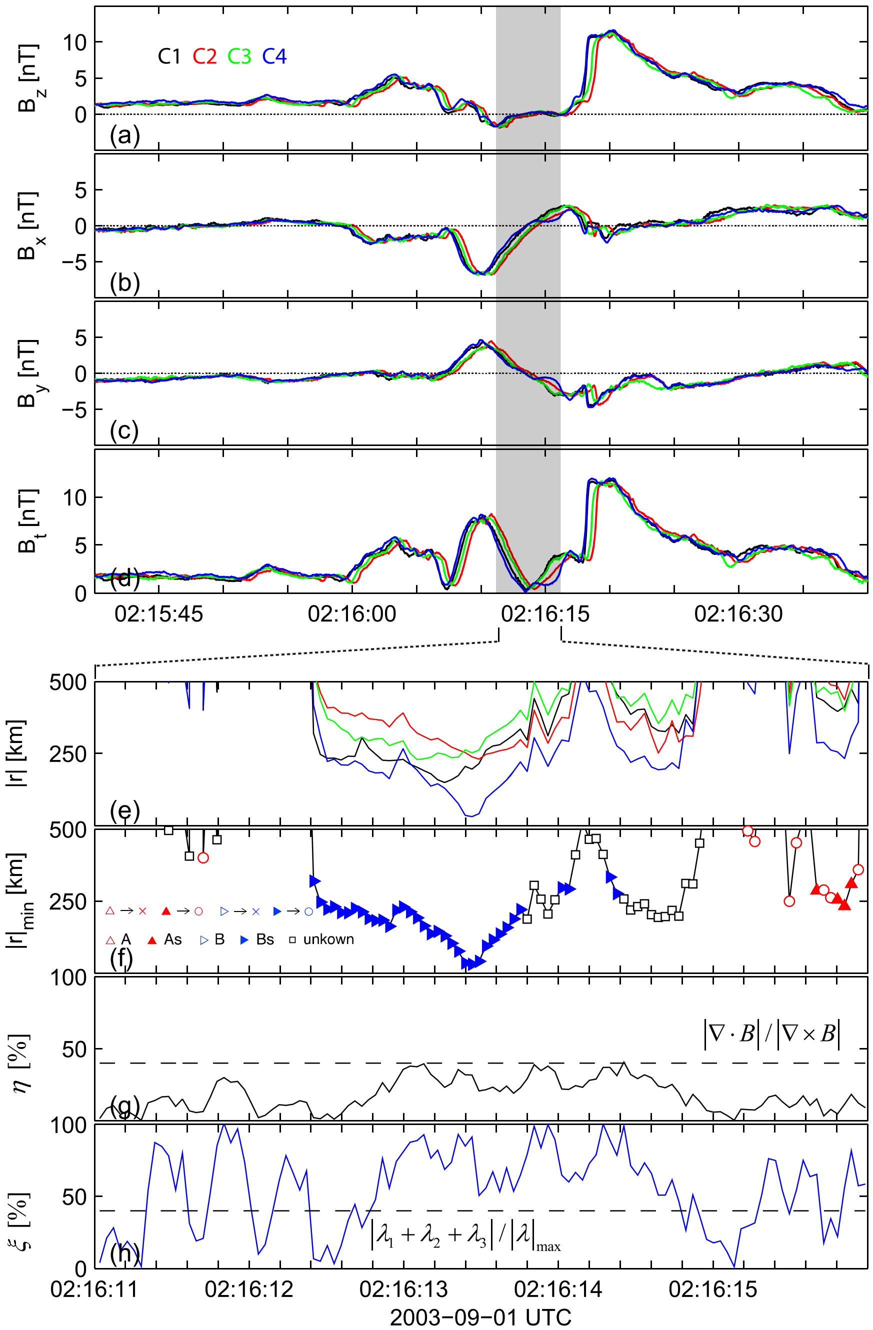

Figure 2. *Cluster* observations of magnetic null in the flux rope ahead of the RF: (a) magnetic field B_z component; (b) magnetic field B_x component; (c) magnetic field B_y component; (d) the strength of the magnetic field; (e) null-SC distance; (f) the minimum null-SC distance with null types labeled; (g), (h) two parameters, η and ξ, for quantifying the quality of the FOTE results. The dashed lines represent the zero levels of magnetic field components.

10:19:13.70–10:19:14.10 UT (Figure 3(e)). From 10:19:12.45 to 10:19:12.85 UT, the minimum distance between the null and spacecraft approaches 67 km ($\sim$0.13 d_i), and the null presented steady Bs or O types with small values of η and ξ, thus we treat the Bs/O null as reliable. Based on its duration ($\sim$0.4 s), its spatial scale was $\sim$96.4 km or equivalently 0.19 d_i. From 10:19:12.90 to 10:19:13.35 UT, the minimum distance between the null and spacecraft approaches 41 km ($\sim$0.08 d_i), and the null steadily presents As types with the parameters $\eta < 40\%$ and $\xi < 40\%$. Thus we also treat the As null as reliable. Considering its duration ($\sim$0.45 s), its spatial scale was $\sim$108 km or equivalently 0.21 d_i. From 10:19:13.70 to 10:19:14.10 UT, the minimum distance between the null and spacecraft approaches 256 km ($\sim$0.5 d_i), and the identified null presents steady Bs types with the parameters η and ξ being almost zero. Therefore, we also treat this As null as reliable. Based on its duration ($\sim$0.4 s), its spatial scale was 96.4 km ($\sim$0.19 d_i). Note that the multiple nulls in this region all have scale well below ion inertial length, therefore existence of these small-scale structures in the front edge of the magnetic flux rope may account for the distinction in observations by the four spacecraft. Such small-scale null structure can be further investigated using data from the recently launched Magnetospheric

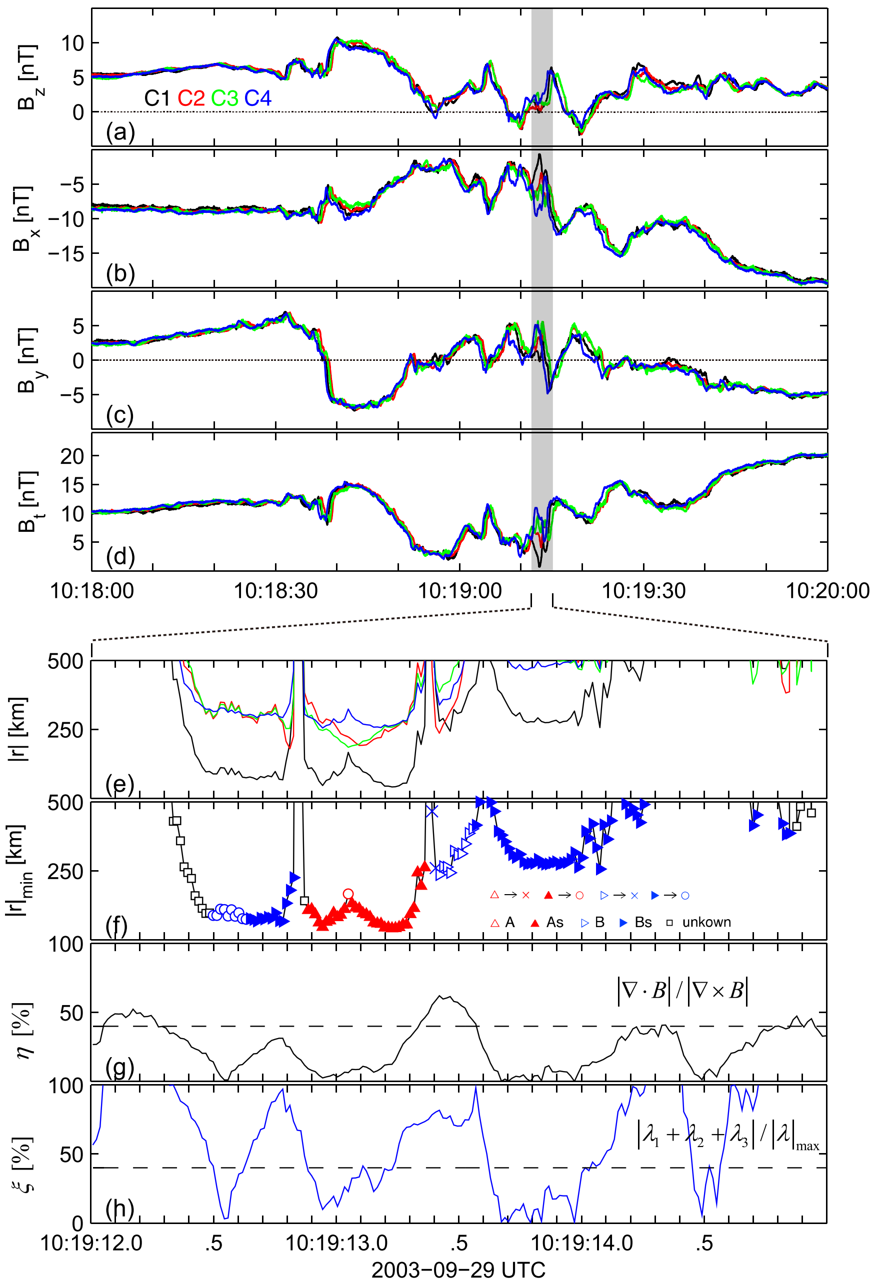

Figure 3. *Cluster* observations of multiple magnetic nulls in the flux rope behind the RF: (a) magnetic field B_z component; (b) magnetic field B_x component; (c) magnetic field B_y component; (d) the strength of the magnetic field; (e) null-SC distance; (f) the minimum null-SC distance with null types labeled; (g), (h) two parameters, η and ξ, for quantifying the quality of the FOTE results. The dashed lines represent the zero levels of magnetic field components.

Multiscale (MMS) mission (Burch et al. 2016) which has a small separation down to electron inertial length. We intend to focus on this issue in the future.

To investigate whether these RF-associated magnetic nulls show typical features predicated by theoretical models (Parnell et al. 1996), we use the FOTE method (Fu et al. 2015) to reconstruct their topology. During the construction, the eigenvector coordinate system (e_1, e_2, e_3) obtained from the Jacobian matrix ∇B is established (Fu et al. 2016). The reconstructed topologies of these magnetic nulls are shown in Figure 4. As can be seen, the reconstructed 3D topologies in Figures 4(a)–(c) are well consistent with theoretical models (Lau & Finn 1990; Parnell et al. 1996; Fu et al. 2017). In Figures 4(d)–(f), the "spiral" feature of the null is clear, and these spiral nulls turn into magnetic islands when we look along the direction (e_1, 0, 0). Constructions of the topologies of these magnetic nulls further confirm the reliability of FOTE results. Interestingly, we find the As null in the dip region ahead of the RF is significantly stretched in the $\pm e_3$ direction (Figure 4(d)), possibly due to compression between the RF and the ambient plasma; the Bs null in the magnetic flux rope before the RF (Figure 4(e)) does not display such feature, possibly because no compression occurs near these structures.

4. Conclusions

In this study, we present for the first time the observational evidence for the occurrence of magnetic nulls associated with RFs, by using the FOTE method and *Cluster* measurements. We find that the dip region ahead of RF and the nearby

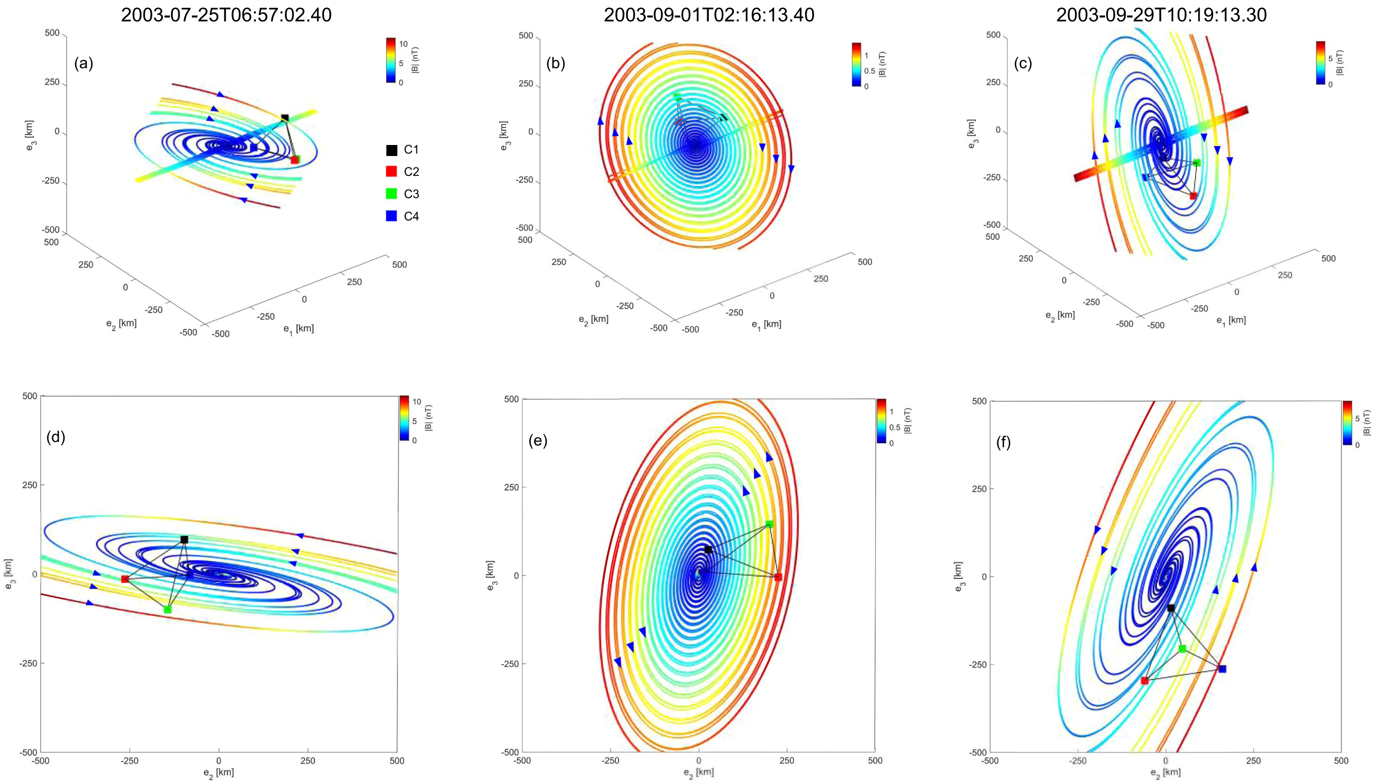

Figure 4. Topology of magnetic nulls associated with RFs. Data are presented in the eigenvector coordinate system (e_1, e_2, e_3). Reconstructions are based on FOTE tracing method. (a) The 3D magnetic-field topology around *Cluster* at 06:57:02.40 UT, 2003 July 25; it corresponds to the As type null in the dip region ahead of the RF; (d) A 2D view, along the direction (e1, 0, 0), of this topology. (b) The 3D magnetic-field topology around *Cluster* at 02:16:13.40 UT, 2003 September 01; it corresponds to the Bs type null in the flux rope before the RF; (e) A 2D view, along the direction (e1, 0, 0), of this topology. (c) The 3D magnetic-field topology around *Cluster* at 10:19:13.30 UT, 2003 September 29; it corresponds to the As type null in the magnetic flux rope behind the RF; (f) A 2D view, along the direction (e_1, 0, 0), of this topology.

magnetic flux ropes around RF can become host to magnetic nulls. The observed magnetic nulls are all spiral types, and the reconstructed topologies of these spiral nulls are well consistent with theoretical models. Our results confirm the existence of magnetic nulls around RFs and may shed new lights on the study of RF dynamics. A statistical investigation of properties of magnetic nulls associated with RF will be performed using MMS data in the future.

We thank *Cluster* Science Archive (http://www.cosmos.esa.int/web/csa) for providing the data for this study. We acknowledge the financial support by NSFC grants 41574153, 41431071, and the ISSI team "Magnetic Topology Effects on Energy dissipation in Turbulent Plasma."

ORCID iDs

C. M. Liu https://orcid.org/0000-0002-9705-5387
Y. Xu https://orcid.org/0000-0003-1863-7280

References

Angelopoulos, V., Runov, A., Zhou, X.-Z., et al. 2013, Sci, 341, 1478
Burch, J. L., Moore, T. E., Torbert, R. B., & Giles, B. L. 2016, SSRv, 199, 5
Cao, J. B., Ma, Y. D., Parks, G., et al. 2006, JGR, 111, A04206
Chen, X. H., Fu, H. S., Liu, C. M., et al. 2018, ApJ, 852, 17
Dalla, S., & Browning, P. K. 2006, ApJL, 640, L99
Deng, X. H., Zhou, M., Li, S. Y., et al. 2009, JGR, 114, A07216
Divin, A., Khotyaintsev, Y. V., Vaivads, A., et al. 2015, JGRA, 120, 2675
Eastwood, J. P., Phan, T. D., Øieroset, M., & Shay, M. A. 2010, JGR, 115, A08215
Eriksson, E., Vaivads, A., Khotyaintsev, Y. V., et al. 2015, GeoRL, 42, 6883
Fu, H. S., Cao, J. B., Cully, C. M., et al. 2014, JGRA, 119, 9089
Fu, H. S., Cao, J. B., Khotyaintsev, Y. V., et al. 2013a, GeoRL, 40, 6023
Fu, H. S., Cao, J. B., Vaivads, A., et al. 2016, JGRA, 121, 1263
Fu, H. S., Khotyaintsev, Y. V., André, M., Vaivads, A., et al. 2011, GeoRL, 38, L16104
Fu, H. S., Khotyaintsev, Y. V., Vaivads, A., et al. 2012a, GeoRL, 39, L10101
Fu, H. S., Khotyaintsev, Y. V., Vaivads, A., et al. 2012b, JGR, 117, A12221
Fu, H. S., Khotyaintsev, Y. V., Vaivads, A., et al. 2012c, GeoRL, 39, L06105
Fu, H. S., Khotyaintsev, Y. V., Vaivads, A., et al. 2013b, NatPh, 9, 426
Fu, H. S., Vaivads, A., Khotyaintsev, Y. V., et al. 2015, JGRA, 120, 3758
Fu, H. S., Vaivads, A., Khotyaintsev, Y. V., et al. 2017, GeoRL, 43, 37
Hasegawa, H., Wang, J., Dunlop, M. W., et al. 2010, GeoRL, 37, L16101
He, J.-S., Zong, Q.-G., Deng, X.-H., et al. 2008, GeoRL, 35, L14104
Huang, S. Y., Fu, H. S., Yuan, Z. G., et al. 2015a, JGRA, 120, 4496
Huang, S. Y., Zhou, M., Yuan, Z. G., et al. 2015b, JGRA, 120, 6188
Khotyaintsev, Y. V., Cully, C. M., Vaivads, A., et al. 2011, PhRvL, 106, 165001
Lapenta, G., Goldman, M., Newman, D., et al. 2014, PhPl, 21, 055702
Lapenta, G., Markidis, S., Goldman, M. V., & Newman, D. L. 2015, NatPh, 11, 690
Lau, Y. T., & Finn, J. M. 1990, ApJ, 350, 672
Liu, C. M., Fu, H. S., Cao, J. B., et al. 2017a, GeoRL, 44, 10116
Liu, C. M., Fu, H. S., Vaivads, A., et al. 2018, GeoRL, 45, 556
Liu, C. M., Fu, H. S., Xu, Y., et al. 2017b, JGRA, 122, 594
Liu, C. M., Fu, H. S., Xu, Y., et al. 2017c, GeoRL, 44, 6492
Lu, S., Lu, Q. M., Lin, Y., et al. 2015, JGRA, 120, 6286
Nakamura, R., Baumjohann, M., Klecker, B., et al. 2002, GeoRL, 29, 1942
Øieroset, M., Lin, R. P., Phan, T. D., et al. 2002, PhRvL, 89, 195001
Øieroset, M., Phan, T. D., Fujimoto, M., et al. 2001, Natur, 412, 414
Olshevsky, V., Deca, J., Divin, A., et al. 2016, ApJ, 819, 52
Olshevsky, V., Divin, A., Eriksson, E., et al. 2015, ApJ, 807, 155
Olshevsky, V., Lapenta, G., & Markidis, S. 2013, PhRvL, 111, 045002
Parnell, C. E., Maclean, R. C., & Haynes, A. L. 2010, ApJL, 725, L214
Parnell, C. E., Neukirch, T., Smith, J. M., & Priest, E. R. 1997, GApFD, 84, 245
Parnell, C. E., Smith, J. M., Neukirch, T., & Pries, E. R. 1996, PhPl, 3, 759

Petkaki, P., & MacKinnon, A. L. 2007, A&A, 472, 623
Pontin, D. I., & Galsgaard, K. 2007, JGR, 112, A03103
Pontin, D. I., Hornig, G., & Priest, E. R. 2005, GApFD, 99, 77
Priest, E. R., & Titov, V. S. 1996, RSPTA, 354, 2951
Pritchett, P. L., Coroniti, F. V., & Nishimura, Y. 2014, JGRA, 119, 4723
Runov, A., Angelopoulos, V., Sitnov, M. I., et al. 2009, GeoRL, 36, L14106
Sitnov, M. I., Swisdak, M., & Divin, A. 2009, JGR, 114, A04202
Titov, V. S., Mikić, Z., Török, T., et al. 2017, ApJ, 845, 141
Wang, J., Cao, J. B., Fu, H. S., et al. 2017, JGRA, 122, 185
Wyper, P. F., & Pontin, D. I. 2014a, PhPl, 21, 102012
Wyper, P. F., & Pontin, D. I. 2014b, PhPl, 21, 082114
Xiao, C. J., Wang, X. G., Pu, Z. Y., et al. 2006, NatPh, 2, 478
Xu, Y., Fu, H. S., Liu, C. M., & Wang, T. Y. 2018, ApJ, 853, 11
Yamada, M., Kulsrud, M. R., & Ji, H. 2010, RvMP, 82, 603
Yao, Z. H., Rae, I. J., Guo, R. L., et al. 2017, JGRA, 122, 4335
Zhou, M., Ashour-Abdalla, M., Deng, X. H., et al. 2009, GeoRL, 36, L20107